ICJK

Journal of Advanced Materials Research
http://dx.doi.org/10.62762/JAMR.2026.419536

RESEARCH ARTICLE

Synergistic Optoelectronic Engineering of Dual-Layer PEDOT: PSS Hole Transport Layers for High-Performance Organic/Silicon Heterojunction Solar Cells

Sami Iqbal[1,2,3,*], **Fahim Ullah**[1,2], **Mazhar Iqbal**[1,3], **Zongru Yang**[4] **and Yi Yang**[4]

[1] Carium Innovation Technology Development Company Pvt Ltd, Islamabad 44000, Pakistan
[2] College of Metallurgy and Energy Engineering, Kunming University of Science and Technology, Kunming 650093, China
[3] Enfiniti Innovate New Technology Development Co., Ltd, Nanjing 210000, China
[4] Joint International Research Laboratory of Information Display and Visualization, School of Electronic Science and Engineering, Southeast University, Nanjing 210096, China

Abstract

Poly(3,4-ethylenedioxythiophene):poly(styrene sulfonate) (PEDOT:PSS)/silicon (Si) hybrid heterojunction solar cells have attracted considerable interest because of their potential for high efficiency, low material cost, and simple fabrication. Their wider adoption, however, is limited by a restricted spectral response and by suboptimal charge transfer at the organic/inorganic interface. Here we address these limitations with a dual-layer PEDOT:PSS (PH1000) film in which ethylene glycol (EG) and dimethyl sulfoxide (DMSO) are added to the bottom and top layers, respectively. The bilayer is designed to tune the optical and electronic properties of the hole transport layer, aiming at small optical losses and better carrier extraction at the organic/inorganic interface. The optimized device, with a total PEDOT:PSS thickness of $\leq$ 150 nm, shows an open-circuit voltage (V_{oc}) of 605 mV, a short-circuit current density (J_{sc}) of 18.55 mA cm^{-2}, and a fill factor (FF) of 62.03%, giving a power conversion efficiency (PCE) of 6.96%, a relative improvement of 112.8% over the single-layer reference (3.27%). Kelvin probe force microscopy (KPFM), atomic force microscopy (AFM) and transmittance measurements indicate a uniform surface potential, a smooth film and only a small optical penalty. These results point to the dual-layer PEDOT:PSS architecture as a practical route to better interfacial charge transport in low-cost hybrid solar cells.

Keywords: hole transport layer, optical absorption, charge extraction, interface engineering.

Submitted: 05 August 2026
Revised: 26 October 2026
Accepted: 02 November 2026
Published: 25 November 2026

Vol. 3, **No.** 1, 2027.
10.62762/JAMR.2026.419536

***Corresponding author:**
✉ Sami Iqbal
dr.samiiqbal@outlook.com

Citation
Iqbal, S., Ullah, F., Iqbal, M., Yang, Z., & Yang, Y. (2026). Synergistic Optoelectronic Engineering of Dual-Layer PEDOT: PSS Hole Transport Layers for High-Performance Organic/Silicon Heterojunction Solar Cells. *Journal of Advanced Materials Research*, 3(1), 1–13.

© 2026 by the Authors. Published by Institute of Central Computation and Knowledge. This is an open access article under the CC BY license (https://creativecommons.org/licenses/by/4.0/).

1 Introduction

The search for efficient, low-cost organic/n-Si hybrid heterojunction solar cells has driven extensive work on materials and device structures that balance performance and cost. Poly(3,4-ethylenedioxythiophene):poly(styrene sulfonate) (PEDOT:PSS) can reach high conductivity when treated with co-solvents [1], and heterojunctions formed between PEDOT:PSS and crystalline n-type silicon (c-Si or n-Si) combine the advantages of organic and silicon-based photovoltaics [2]. PEDOT:PSS is a conductive polymer with high optical transparency, flexibility and good processability, and its conductivity can be raised strongly by structural control [3]. This makes it a suitable hole transport layer (HTL) in silicon heterojunction (SHJ) solar cells, where Si/PEDOT:PSS hybrid cells with efficiencies above 13% have been demonstrated [4]. It offers a low-cost, adaptable HTL that can be integrated with conventional silicon technology [5–7]. To optimize the interface, in particular to reduce recombination and maximize carrier collection, the thickness and deposition method of PEDOT:PSS have to be considered. Here we investigate a dual-layer PEDOT:PSS structure with a total thickness of ≤ 150 nm, aiming to balance conductivity and transparency at the device interface. The energy alignment of PEDOT:PSS with n-Si favors hole transport while limiting electron leakage, as the majority- and minority-carrier barriers at the Si/organic interface determine the device behavior [8]. The work function of PEDOT:PSS is about 5.0 eV, close to the valence band edge of n-Si, which allows selective hole extraction. Thin films can be cast from aqueous solution, which enables inexpensive, large-scale fabrication [9]; PEDOT:PSS/n-Si cells on textured surfaces with solution-processed AgNW electrodes have also been reported [10]. Even so, device performance depends strongly on the PEDOT:PSS thickness. A thin film with incomplete coverage leaves defects and increases recombination at the PEDOT:PSS/n-Si interface [11], and the SiO_x interlayer at this interface must be controlled for the same reason [12], whereas an excessively thick layer reduces light transmission and limits the photocurrent. The optimal thickness is therefore critical: about 140 nm has been reported for a single-layer film on polished Si [13], and placing PEDOT:PSS at the rear to avoid parasitic absorption has also been explored [14]. Beyond thickness, depositing the film in two steps may improve its morphology and interfacial contact. Film robustness is also relevant to device stability [15], and pinhole formation and roughness at the interface strongly influence junction quality [16], and the surface structure also affects carrier separation and collection [17]. A dual-layer structure aims to improve light absorption without sacrificing electrical conductivity: light must reach the Si absorber while hole transport stays efficient, as required for high-efficiency planar Si/organic cells, including those with V_{oc} up to 645 mV and efficiencies of 12.6% [18, 19]. A film thickness of about 150 nm has been optimized for planar cells [20]. In a bilayer, the first deposition is expected to give a smooth interface, and the second to cover residual roughness or uncovered areas.

Interface energetics and transport can be tuned further by secondary doping of PEDOT:PSS. Additives such as ethylene glycol (EG) and dimethyl sulfoxide (DMSO) markedly raise the conductivity of PEDOT:PSS films [21, 22], and about 5 wt% DMSO improves the film structure, surface and interface in hybrid solar cells [23], which benefits the power conversion efficiency (PCE). By weakening the Coulombic interaction between PEDOT and PSS chains, they open the film structure and ease charge transport [24]. Controlled doping and thickness optimization balance conductivity and transparency, which matters for device efficiency [20], and recent progress in organic-silicon hybrid cells has been reviewed [25]. A dual-layer structure can build on this. PEDOT:PSS is hygroscopic and acidic, so environmental stability is a concern for PEDOT:PSS/n-Si cells, as also seen in their light-induced stability [15]. Double-layered PEDOT:PSS films have been reported to induce a strong inversion layer in the Si and so to improve junction quality [26]. Keeping the thickness uniform over large areas is a further challenge. Printing and coating techniques, including slot-die coating, have been reviewed for large-area polymer solar cells [27], and spray-coated high-conductivity PEDOT:PSS films have been demonstrated [28]. These routes offer scalable, low-cost production. Together with material modification, advances in deposition technology open new routes to higher PCE at low fabrication cost.

Dual-layer deposition, in which two PEDOT:PSS layers are deposited in sequence, is a possible way to optimize the thickness while retaining efficient charge transfer. Studies of Si/organic heterojunctions have reported that better junction quality and interface passivation reduce surface recombination and series resistance [29]. A bilayer allows each layer to be tuned separately: the conductivity of PEDOT:PSS can be raised to metallic levels by treatment with organic salts [30], and

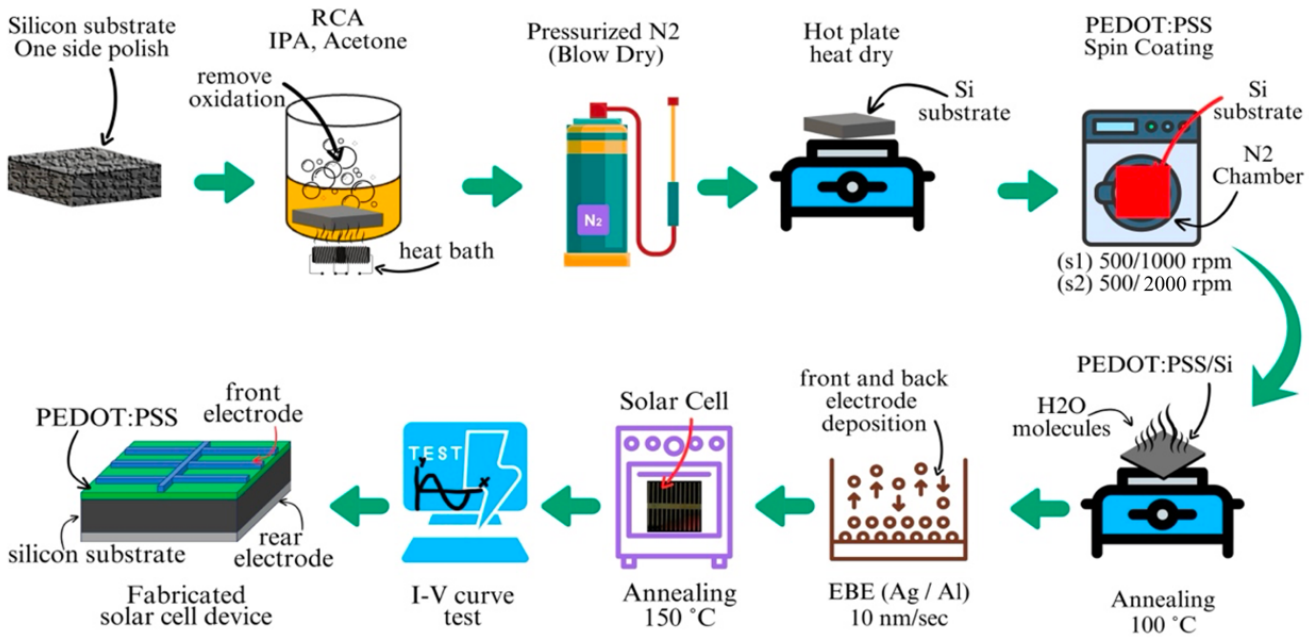

Figure 1. Graphical abstract of the PEDOT:PSS/n-Si solar cell fabrication procedure. Silicon substrates are prepared by the RCA clean process (IPA, acetone and DI water), followed by an HF rinse with DI water, blow drying with N_2, and heat drying on a hot plate. The PEDOT:PSS with EG 7% and DMSO 5% was prepared by magnetic stirring. The PEDOT:PSS was spin-cast onto the n-Si substrate in two steps: s1 (500/1000 rpm, EG 7%) and s2 (500/1500 rpm, DMSO 5%). Electrodes are deposited by electron beam evaporation (EBE): 300 nm Ag (front) and 500 nm Al (back).

thin organic layers on Si have given record hybrid-cell efficiencies [31]. A high-conductivity formulation can therefore be combined with a second layer that sets the target thickness while preserving carrier transport. Interface engineering and carrier-barrier design raise the open-circuit voltage (V_{oc}) and short-circuit current density (J_{sc}) of hybrid Si/organic cells [8, 32]. A PEDOT:PSS thickness of $\leq$ 150 nm is expected to balance light absorption, hole transport and recombination losses, and thus to support a high V_{oc} and J_{sc}. A dual-layer process may also overcome the difficulty of forming uniform films on silicon with a single deposition, especially above 100 nm. By stacking films with controlled interfacial properties, it aims to improve surface passivation and interfacial charge dynamics between PEDOT:PSS and n-Si, both of which determine the PCE. The conductivity of PEDOT:PSS is central to its role as an HTL and can be adjusted through the PEDOT:PSS ratio, secondary dopants or annealing. High-boiling-point solvents such as DMSO or EG raise the conductivity by modifying the polymer structure [33]. This improves carrier extraction and lowers the sheet resistance of the device, and minimizing film defects is equally important for high efficiency [11].

Interface engineering between PEDOT:PSS and n-Si is also needed to reduce recombination losses. Low interface recombination is required to reach the high V_{oc} potential of organic-silicon heterojunctions [34]. Surface treatments such as an ultrathin oxide layer or self-assembled monolayers (SAMs) can be used to this end. Passivating interlayers reduce the density of interfacial defects and thus aid charge extraction and separation at the heterojunction. Combining such interlayers with a bilayer PEDOT:PSS film is a logical next step [26]. The dual-layer architecture is therefore a promising approach to the limits of single-layer deposition. Part of this concept has been described in earlier reports [35, 36]. The present work differs in using a different secondary dopant in each layer (EG in the bottom layer, DMSO in the top layer) and in examining the surface-potential uniformity by KPFM. This work compares a dual-layer EG/DMSO PEDOT:PSS HTL ($\leq$ 150 nm) with a single-layer DMSO reference and examines their optical, electrical, morphological and surface-potential properties. Such a bilayer could improve the commercial viability of PEDOT:PSS/n-Si solar cells by offering an adaptable, low-cost route to interface engineering.

2 Experimental Process

2.1 Materials

A highly conductive PEDOT:PSS aqueous solution with a PEDOT to PSS ratio of 1:2.5 (Heraeus, Clevios

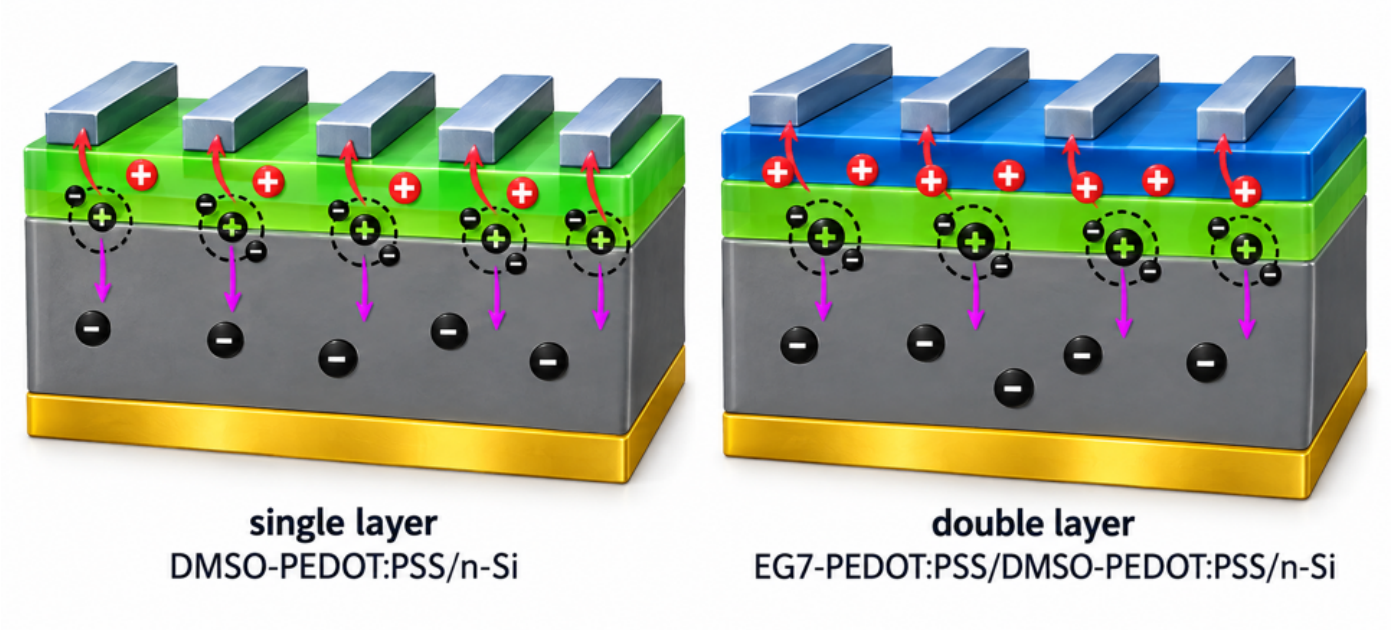

Figure 2. Cross-sectional schematic illustration of PEDOT:PSS/n-Si solar cells with various treatments. (a) Single-layer DMSO (5 wt%) treated PEDOT:PSS/n-Si device. (b) Dual-layer PEDOT:PSS with EG 7% and DMSO 5%, respectively, intended to improve junction formation, carrier separation and transport, leading to a larger V_{oc} and higher efficiency.

PH 1000) was used. Triton X-100 (TX) was purchased from Sigma-Aldrich, DMSO from Sartorius, and ethylene glycol from Univar Solutions. Silver (Ag), aluminum (Al) and silicon substrates were obtained commercially, and acetone, isopropyl alcohol and DI water for the RCA cleaning were purchased locally. All materials were used as received, without further purification.

2.2 EG Doping of PEDOT:PSS

A 20 mL PEDOT:PSS (PH1000) solution was mixed with 7 wt% ethylene glycol (EG) and 0.1 wt% Triton X-100 and stirred magnetically at 1000 rpm to obtain a homogeneous solution (stirring time not stated). The surfactant improves wetting on the Si surface, and EG raises the conductivity of the film.

2.3 DMSO Doping of PEDOT:PSS

A 20 mL PEDOT:PSS (PH1000) solution was mixed with 5 wt% DMSO and stirred magnetically at 600 rpm until fully mixed, giving a well-dispersed solution. Both additives raise the conductivity of the film, which benefits charge transport in the PEDOT:PSS/n-Si device.

3 Fabrication Procedures

The RCA cleaning process was used to clean n-type, single-side polished Czochralski (CZ) monocrystalline Si (100) wafers of 200 $\pm$ 10 μm thickness and 0.05–0.1 Ω cm resistivity. The native oxide was removed by immersion in 5 wt% hydrofluoric acid (HF), and the wafers were dried with pressurized N_2. The PEDOT:PSS solution with 7 wt% EG and 0.1 wt% Triton X-100 was filtered through a 0.45 μm filter and spin-coated onto the Si substrates at S1-500/S2-2000 rpm for 30 s, followed by annealing on a hotplate at 100 °C for 2 min in ambient air, which gave a uniform thin film of $\approx$ 90 nm thickness.

A second layer of PEDOT:PSS (Heraeus, Clevios PH 1000) containing 5 wt% DMSO was then spin-coated onto the EG7-PEDOT:PSS layer at 500/1500 rpm and annealed on a hotplate at 120 °C for 5 min in ambient air. The total thickness of the dual-layer EG7-PEDOT:PSS/DMSO5-PEDOT:PSS film is $\leq$ 150 nm. A 300 nm thick Ag grid top electrode and a 500 nm thick Al back electrode (ohmic contact) were deposited by electron beam evaporation (EBE). The complete experimental procedure is shown in Figure 1.

4 Device Characterization

The samples were examined by scanning electron microscopy (SEM) using a Zeiss Ultra Plus (Gemini) field-emission microscope with an Oxford Instruments X-Max detector (Abingdon, UK). The front-surface reflectance was measured with an IdeaOptics PG2000-Pro EX fiber-optic spectrometer (IdeaOptics Instruments, Shanghai, China). AFM topography images were recorded with a Bruker NanoScope V

Table 1. Photovoltaic performance parameters of PEDOT:PSS/Si hybrid solar cells with single-layer (SL) and dual-layer (DL) device architectures.

Device Structure	V_{oc} [mV]	J_{sc} [mA cm^{-2}]	FF [%]	PCE [%]	EQE [%]
DMSO [5 wt%]	475.7	13.43	51.17	3.27	50.36
EG:DMSO [7 wt% - 5 wt%]	605.0	18.55	62.03	6.96	53.07
Improvement	+27.2%	+38.1%	+21.2%	+112.8%	+5.4%

Multimode system in ScanAsyst mode (Billerica, MA, USA). The current density–voltage (J–V) characteristics, from which V_{oc}, J_{sc}, fill factor (FF) and PCE were extracted, were measured under simulated solar illumination of 100 mW cm^{-2} (AM 1.5G, xenon lamp, Oriel) with a Crowntech solar simulator (IV test station 6000AAA, Macungie, PA, USA) and a 1×1 cm^2 mask. The irradiation intensity was calibrated with a standard silicon reference cell, and the temperature was kept at 25 ± 0.5 °C during the measurement. The external quantum efficiency (EQE) was measured with a Crowntech Qtest station 2000AD (xenon light source, spot size 1×2.5 mm^2) calibrated with a silicon photodetector.

5 Results and Discussion

Figure 2 shows the schematics of the two fabricated devices: (a) PEDOT:PSS treated with 5 wt% DMSO, and (b) a double-layer device whose first PEDOT:PSS layer contains 7 wt% EG and whose second layer contains 5 wt% DMSO. In Figure 2(b), the EG layer mainly provides smoothing and adhesion. EG acts as a secondary dopant that raises the conductivity and improves film formation, giving a homogeneous, defect-free coating that improves the contact between PEDOT:PSS and the Si substrate. The DMSO layer is intended to maximize conductivity: DMSO promotes partial removal and phase separation of insulating PSS chains, which improves the electrical properties of PEDOT:PSS. The bilayer thus combines the complementary effects of EG and DMSO in one HTL.

The dual-layer deposition addresses charge transfer and recombination. The first layer forms a smooth, continuous contact and lowers the density of recombination centers at the PEDOT:PSS/Si interface, which is critical for a high V_{oc}. The second, more conductive layer raises the carrier mobility and aids hole transport from silicon to the anode. A total thickness of ≤ 150 nm is expected to give a favorable electric-field distribution in the HTL and to reduce resistive losses (not verified by simulation here). The first (EG 7 wt%) layer also acts as a buffer that smooths surface defects of the wafer and promotes adhesion to n-Si, which matters for long-term stability; the second (DMSO 5 wt%) layer maximizes conductivity while preserving the first layer. Each layer thus contributes its own function.

Figure 3 compares single- and double-layer PEDOT:PSS/n-Si cells (see also Table 1). Figure 3(a) shows the device structure, with PEDOT:PSS as the HTL on n-Si. Figure 3(b) shows the EQE spectra: the double-layer device has a higher EQE over 400–900 nm, with a maximum of 53.07% (Table 1). The dark J–V curves in Figure 3(c) indicate a lower reverse saturation current and better rectification for the double-layer device, consistent with reduced recombination. Under illumination (Figure 3(d)), the double-layer device reaches a higher J_{sc} and V_{oc} and hence a higher PCE, in line with a lower series resistance and better surface passivation. Overall, the double-layer structure improves the interfacial properties, lowers recombination and raises the spectral response relative to the single-layer cell.

Figure 4(a) is a cross-sectional SEM image of the DL-PEDOT:PSS/n-Si device with its two distinct layers, EG-PEDOT:PSS and DMSO-PEDOT:PSS; this structure gives better film uniformity and interfacial coverage. Figure 4(b) shows the SL-PEDOT:PSS/n-Si device, whose coating is thinner and less uniform; such a coating is more prone to interfacial defects and recombination, which lowers the efficiency.

Figure 5(a) shows the bilayer PEDOT:PSS acting as the hole-selective contact on n-Si, and Figure 5(b) the corresponding energy-level diagram, including the work functions of the Ag front contact (4.30 eV) and the Al rear contact (4.28 eV), the HOMO/LUMO levels of both PEDOT:PSS layers, and the band structure of n-Si ($E_c = -4.05$ eV, $E_v = -5.17$ eV, $E_g = 1.12$ eV). This alignment is expected to favor selective hole extraction from n-Si into PEDOT:PSS while suppressing electron transport. The double-layer film thus improves both the physical uniformity and the interfacial electronic properties, which supports the higher device performance.

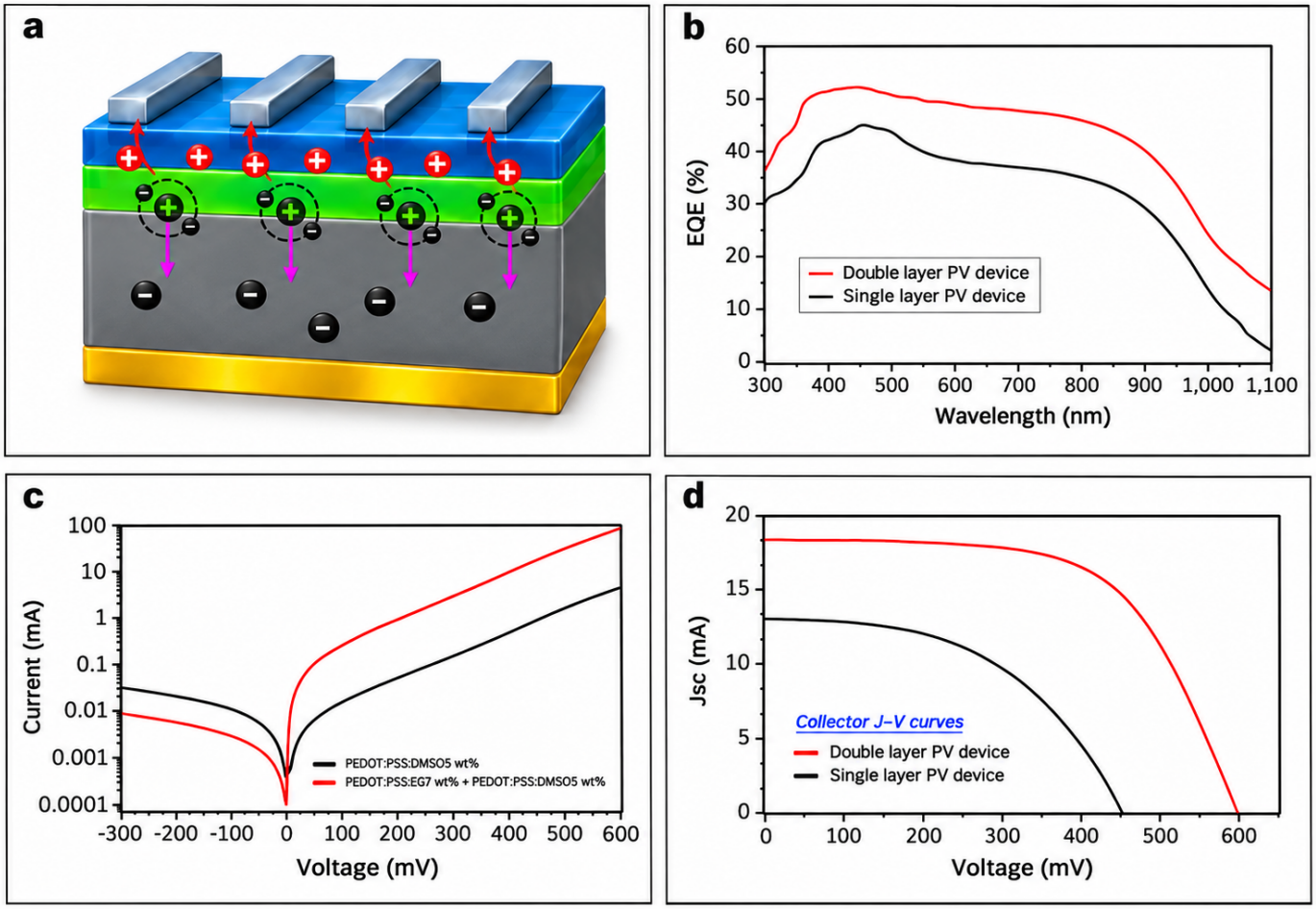

Figure 3. Characterization of PEDOT:PSS/n-Si solar cells, comparing single-layer and double-layer configurations through (a) device schematic, (b) EQE spectra, (c) dark J-V curves and (d) illuminated J-V curves.

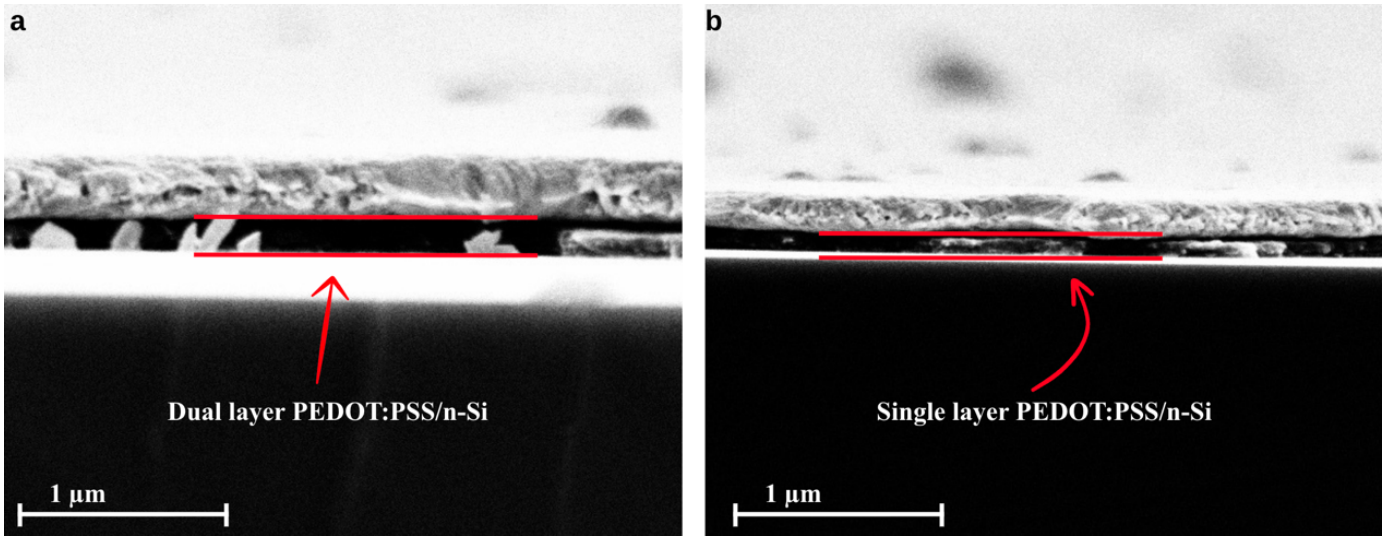

Figure 4. Cross-sectional SEM images of (a) dual-layer PEDOT:PSS/n-Si device and (b) single-layer PEDOT:PSS/n-Si device.

Figure 6 shows the KPFM characterization of the double-layer PEDOT:PSS contact on n-Si: (a) contact potential difference (CPD) map, (b) 3D CPD, (c) CPD distribution, (d) line profiles, (e) work function map and (f) the potential-gradient map $|\nabla V|$. The narrow CPD distribution and the uniform work function map indicate a homogeneous surface potential, and the low $|\nabla V|$ contrast indicates a smooth potential

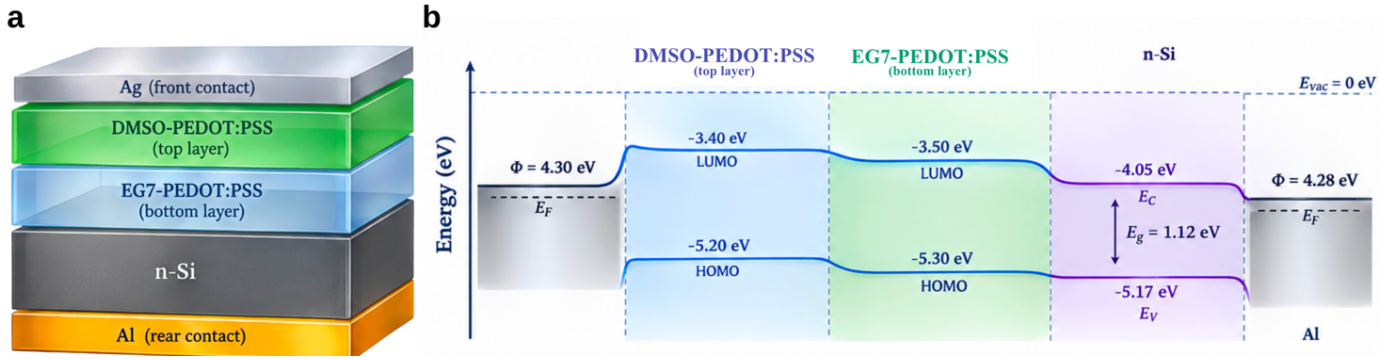

Figure 5. (a) Schematic of the device architecture Ag/DMSO-PEDOT:PSS (top)/EG7-PEDOT:PSS (bottom)/n-Si/Al. (b) Energy-level diagram of the corresponding layers.

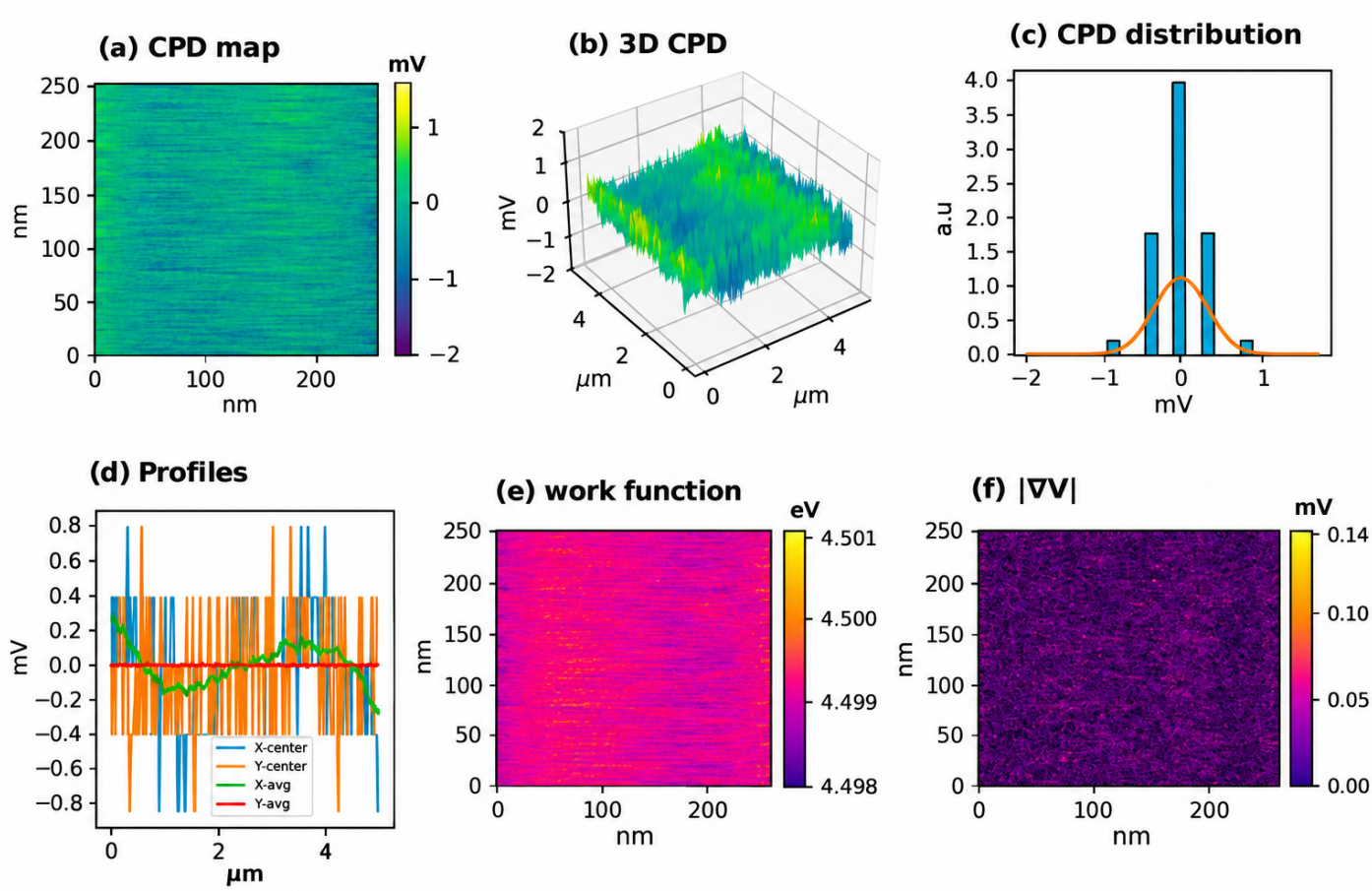

Figure 6. KPFM characterization of the surface: (a) CPD map, (b) 3D CPD, (c) CPD distribution, (d) line profiles, (e) work function map, and (f) potential-gradient map $|\nabla V|$.

landscape without significant local variations. The EG/DMSO bilayer therefore appears to form a uniform hole-selective contact with reduced interfacial inhomogeneity, which is expected to lower interfacial recombination and ease hole extraction, in line with the higher V_{oc}, FF and PCE of the double-layer device.

To check whether the bilayer introduces additional optical losses, UV–Vis transmittance spectra of the single-layer and dual-layer samples were measured (Figure 7). Both show high transmittance in the visible region, with averages of 90% (single layer) and 87% (dual layer) between 400 and 700 nm; at 1000 nm the transmittance falls to 77% and 72%, respectively. The dual-layer sample is slightly less transparent above about 400 nm (it is marginally more transparent below about 350 nm), but this small optical penalty cannot explain the large gain in performance: J_{sc} rose from 13.43 to 18.55 mA cm^{-2}, V_{oc} from 475.7 to 605.0 mV, FF from 51.17% to 62.03%, and PCE from 3.27% to 6.96%.

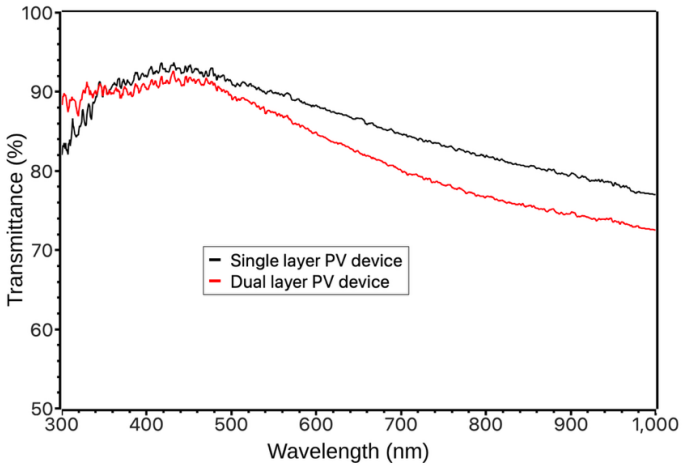

Figure 7. Transmittance spectra of single-layer and dual-layer PEDOT:PSS films in the wavelength range of 300–1000 nm.

The improvement therefore appears to come mainly from electrical effects, such as better hole selectivity, lower interfacial recombination and a more uniform surface potential, which is consistent with the KPFM results.

The surface morphology of the double-layer film was also examined by AFM. In Figure 8(a–e), the 2D and 3D topography images show a smooth, homogeneous surface without visible aggregates, pinholes or large defects. The height histograms are narrow, and the cross-sectional profiles fluctuate by only a few nanometers in both directions, indicating a uniform film with low roughness, as needed for a high-quality heterojunction with n-Si. The arithmetic mean roughness R_a and root-mean-square roughness R_q are 145 nm and 169 nm for the dual-layer PEDOT:PSS/n-Si sample, compared with $R_a = 163$ nm and $R_q = 186$ nm for the single-layer sample. A smooth film minimizes interfacial defects and ensures intimate contact, which eases charge extraction and reduces recombination; this agrees with the KPFM results. Taken together, the AFM, KPFM and UV–Vis data indicate that the bilayer contact keeps good optical transparency while improving charge transport.

6 Conclusion

We have optimized PEDOT:PSS/n-Si hybrid heterojunction solar cells with a dual-layer deposition approach. An EG-doped (7 wt%) bottom layer and a DMSO-doped (5 wt%) top layer with a total thickness of $\leq$150 nm improved charge transfer, reduced recombination and improved the interfacial properties. The EG-doped bottom layer provided surface smoothing and adhesion to the n-Si substrate, and the DMSO-doped top layer raised the conductivity and carrier mobility. In comparison with the single-layer device, the bilayer is expected to lower the series resistance and improve the surface passivation, which supports charge extraction and collection.

The optimized dual-layer device reached $V_{oc} = 605$ mV, $J_{sc} = 18.55$ mA cm^{-2} and FF = 62.03%, giving a PCE of 6.96%, a relative improvement of 112.8% over the single-layer reference (PCE = 3.27%). The EQE rose from 50.36% to 53.07%, indicating a better spectral response. The dark J–V curves of the dual-layer device show a lower reverse saturation current and better rectification, which points to a better junction quality. These results show that interface engineering of the HTL can improve low-cost silicon hybrid solar cells. The absolute PCE reached here is still lower than the 12–14% reported for optimized planar PEDOT:PSS/Si cells [11, 19].

Data Availability Statement

Data will be made available on request.

Funding

This work was supported in part by the Leading-Edge Technology Program of Jiangsu Natural Science Foundation under Grant BK20232001; in part by the National Natural Science Foundation of China under Grant 62275047 and Grant 22102023; in part by the Natural Science Foundation of Jiangsu Province under Grant BK20220816; in part by the Jiangsu Key Science and Technology project under Grant BE2019108; in part by the fellowship of China Postdoctoral Science Foundation under Grant 2022M710672; in part by the Jiangsu NSFC Excellent Postdoctoral funding under Grant 2022ZB78; in part by the Postdoctoral Startup Fund of the School of Material Science and Engineering, Southeast University under Grant 1112002208 and Grant 4012002313.

Conflicts of Interest

Sami Iqbal served as an Editorial Board Member of the *Journal of Advanced Materials Research* at the time of manuscript submission. To ensure the integrity and impartiality of the peer-review process, Sami Iqbal had no involvement in the editorial handling, peer review, or decision-making for this manuscript, which was handled independently by another editor. Sami Iqbal and Mazhar Iqbal are affiliated with Enfiniti Innovate New Technology Development Co., Ltd., Nanjing

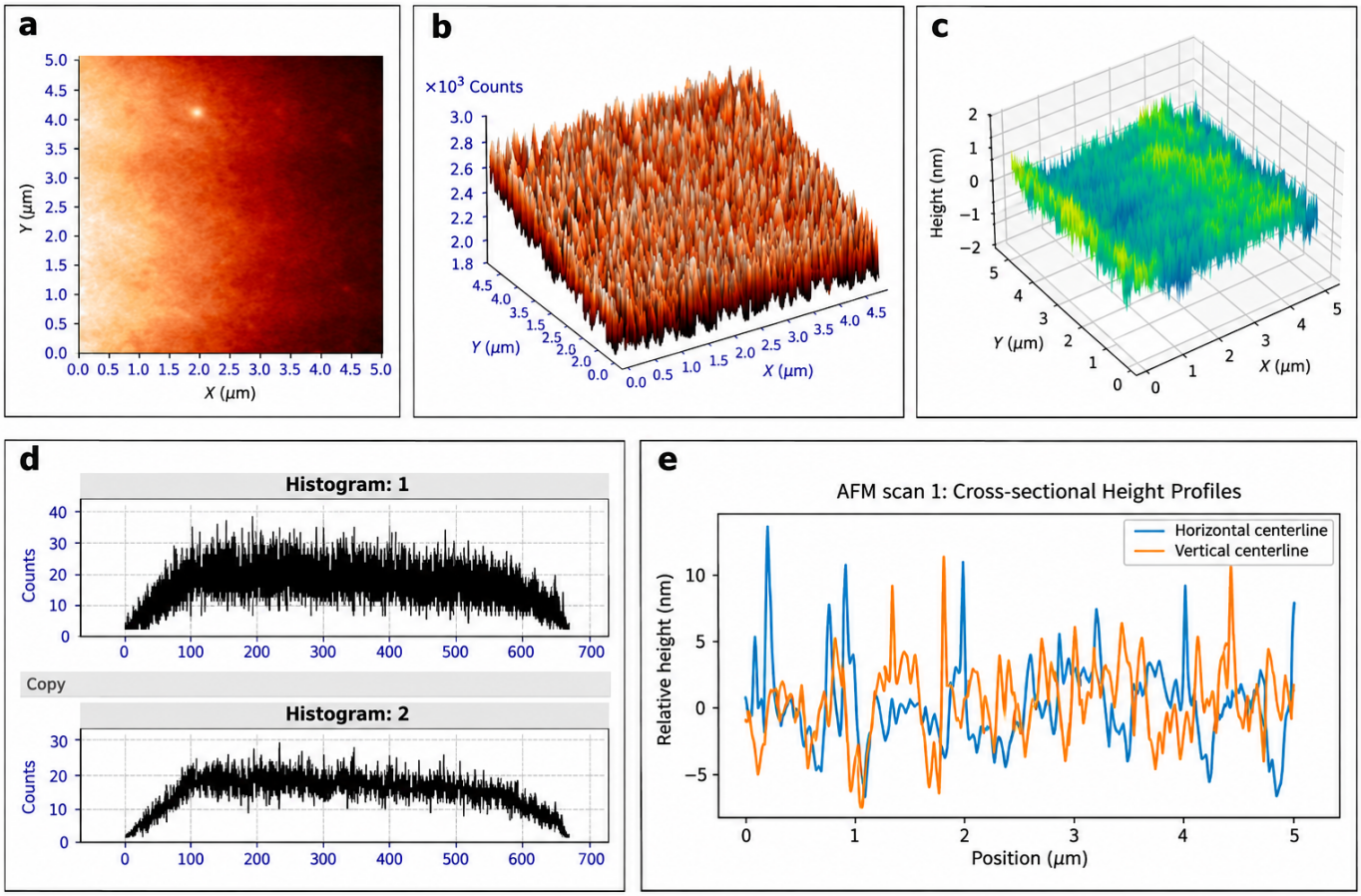

Figure 8. AFM characterization of the double-layer PEDOT:PSS film: (a) 2D topography image, (b) 3D surface plot, (c) 3D surface plot with color-coded height distribution, (d) height histograms, and (e) cross-sectional height profiles.

210000, China. Fahim Ullah is affiliated with Carium Innovation Technology Development Company Pvt Ltd, Islamabad 44000, Pakistan. These affiliations had no influence on the study design, data collection, analysis, interpretation, or decision to publish. The remaining authors declare no conflicts of interest.

AI Use Statement

The authors declare that Google Gemini was used to improve the English wording and flow of the experimental explanations for the convenience of readers. The authors have carefully reviewed, revised, and verified the AI-assisted output and take full responsibility for the content of the manuscript.

Ethical Approval and Consent to Participate

Not applicable.

References

[1] Xia, Y., & Ouyang, J. (2011). PEDOT:PSS films with significantly enhanced conductivities induced by preferential solvation with cosolvents and their application in polymer photovoltaic cells. *Journal of Materials Chemistry, 21*(13), 4927–4936. [CrossRef]

[2] Chen, T., Guo, H., Yu, L., Sun, T., & Yang, Y. (2020). Silicon substrate treated with diluted NaOH aqueous for Si/PEDOT:PSS heterojunction solar cell with performance enhancement. *Energies, 13*(18), 4659. [CrossRef]

[3] Kim, N., Kee, S., Lee, S. H., Lee, B. H., Kahng, Y. H., Jo, Y. R., ... & Lee, K. (2014). Highly conductive PEDOT: PSS nanofibrils induced by solution-processed crystallization. *Advanced materials, 26*(14), 2268-2272. [CrossRef]

[4] Park, K. T., Kim, H. J., Park, M. J., Jeong, J. H., Lee, J., Choi, D. G., ... & Choi, J. H. (2015). 13.2% efficiency Si nanowire/PEDOT: PSS hybrid solar cell using a transfer-imprinted Au mesh electrode. *Scientific Reports, 5*(1), 12093. [CrossRef]

[5] Thomas, J. P., & Leung, K. T. (2016). Mixed co-solvent engineering of PEDOT:PSS to enhance its conductivity and hybrid solar cell properties. *Journal of Materials Chemistry A, 4*(44), 17537–17542. [CrossRef]

[6] Sun, Z., He, Y., Xiong, B., Chen, S., Li, M., Zhou, Y., Zheng, Y., Sun, K., & Yang, C. (2021). Performance-enhancing approaches for PEDOT:PSS-Si

hybrid solar cells. *Angewandte Chemie International Edition, 60*(10), 5036–5055. [CrossRef]

[7] Shen, X., Sun, B., Liu, D., & Lee, S. T. (2011). Hybrid heterojunction solar cell based on organic–inorganic silicon nanowire array architecture. *Journal of the American Chemical Society, 133*(48), 19408-19415. [CrossRef]

[8] Avasthi, S., Lee, S., Loo, Y. L., & Sturm, J. C. (2011). Role of majority and minority carrier barriers silicon/organic hybrid heterojunction solar cells. *Advanced materials, 23*(48), 5762-5766. [CrossRef]

[9] Kirchmeyer, S., & Reuter, K. (2005). Scientific importance, properties and growing applications of poly(3,4-ethylenedioxythiophene). *Journal of Materials Chemistry, 15*(21), 2077–2088. [CrossRef]

[10] Jiang, X., Zhang, P., Zhang, J., Wang, J., Li, G., Fang, X., ... & Chen, X. (2018). High performance of PEDOT: PSS/n-Si solar cells based on textured surface with AgNWs electrodes. *Nanoscale Research Letters, 13*(1), 53. [CrossRef]

[11] Thomas, J. P., & Leung, K. T. (2014). Defect-minimized PEDOT:PSS/planar-Si solar cell with very high efficiency. *Advanced Functional Materials, 24*(31), 4978–4985. [CrossRef]

[12] Zhang, C., Zhang, Y., Guo, H., Jiang, Q., Dong, P., & Zhang, C. (2018). Efficient planar hybrid n-Si/PEDOT:PSS solar cells with power conversion efficiency up to 13.31% achieved by controlling the SiO_x interlayer. *Energies, 11*(6), 1397. [CrossRef]

[13] Punia, U., Kumari, P., Sharma, R. K., Laxmi, S., Srivastava, R., & Srivastava, S. K. (2024). Fabrication of low-cost and efficient PEDOT: PSS-silicon hybrid heterojunction solar cell via tailoring the organic layer thickness. *Journal of Materials Science: Materials in Electronics, 35*(1), 42. [CrossRef]

[14] Zhang, X., Yang, D., Yang, Z., Guo, X., Liu, B., Ren, X., & Liu, S. (2016). Improved PEDOT: PSS/c-Si hybrid solar cell using inverted structure and effective passivation. *Scientific reports, 6*(1), 35091. [CrossRef]

[15] Liu, Q., Ishikawa, R., Funada, S., Ohki, T., Ueno, K., & Shirai, H. (2015). Highly efficient solution-processed poly (3, 4-ethylenedio-xythiophene): poly (styrenesulfonate)/Crystalline–Silicon heterojunction solar cells with improved light-induced stability. *Advanced Energy Materials, 5*(17), 1500744. [CrossRef]

[16] Jäckle, S., Liebhaber, M., Niederhausen, J., Buchele, M., Félix, R., Wilks, R. G., ... & Christiansen, S. (2016). Unveiling the hybrid n-Si/PEDOT: PSS interface. *ACS applied materials & interfaces, 8*(13), 8841-8848. [CrossRef]

[17] Sugano, Y., Sato, K., Fukata, N., & Hirakuri, K. (2017). Improved separation and collection of charge carriers in micro-pyramidal-structured silicon/PEDOT:PSS hybrid solar cells. *Energies, 10*(4), 420. [CrossRef]

[18] He, L., Jiang, C., Wang, H., Lai, D., & Rusli. (2012). High efficiency planar Si/organic heterojunction hybrid solar cells. *Applied Physics Letters, 100*(7), 073503. [CrossRef]

[19] Pietsch, M., Jäckle, S., & Christiansen, S. (2014). Interface investigation of planar hybrid n-Si/PEDOT:PSS solar cells with open circuit voltages up to 645 mV and efficiencies of 12.6%. *Applied Physics A, 115*(4), 1109–1113. [CrossRef]

[20] Iqbal, S., Su, D., Yang, Y., Ullah, F., Zhou, H., Hussain, A., & Zhang, T. (2019). Fabrication of an efficient planar organic-silicon hybrid solar cell with a 150 nm thick film of PEDOT: PSS. *Micromachines, 10*(10), 648. [CrossRef]

[21] Kim, Y. H., Sachse, C., Machala, M. L., May, C., Müller-Meskamp, L., & Leo, K. (2011). Highly conductive PEDOT:PSS electrode with optimized solvent and thermal post-treatment for ITO-free organic solar cells. *Advanced Functional Materials, 21*(6), 1076–1081. [CrossRef]

[22] Lin, Y. J., Ni, W. S., & Lee, J. Y. (2015). Effect of incorporation of ethylene glycol into PEDOT:PSS on electron phonon coupling and conductivity. *Journal of Applied Physics, 117*(21), 215501. [CrossRef]

[23] Mahato, S., Puigdollers, J., Voz, C., Mukhopadhyay, M., Mukherjee, M., & Hazra, S. (2020). Near 5% DMSO is the best: A structural investigation of PEDOT: PSS thin films with strong emphasis on surface and interface for hybrid solar cell. *Applied Surface Science, 499*, 143967. [CrossRef]

[24] Nardes, A. M., Janssen, R. A. J., & Kemerink, M. (2008). A morphological model for the solvent-enhanced conductivity of PEDOT:PSS thin films. *Advanced Functional Materials, 18*(6), 865–871. [CrossRef]

[25] Zhang, T., Iqbal, S., Zhang, X. Y., Wu, W., Su, D., & Zhou, H. L. (2020). Recent advances in highly efficient organic-silicon hybrid solar cells. *Solar Energy Materials and Solar Cells, 204*, 110245. [CrossRef]

[26] Zhu, J., Yang, X., Sheng, J., Gao, P., & Ye, J. (2018). Double-layered PEDOT:PSS films inducing strong inversion layers in organic/silicon hybrid heterojunction solar cells. *ACS Applied Energy Materials, 1*(6), 2874–2881. [CrossRef]

[27] Krebs, F. C. (2009). Fabrication and processing of polymer solar cells: A review of printing and coating techniques. *Solar Energy Materials and Solar Cells, 93*(4), 394–412. [CrossRef]

[28] Tait, J. G., Worfolk, B. J., Maloney, S. A., Hauger, T. C., Elias, A. L., Buriak, J. M., & Harris, K. D. (2013). Spray coated high-conductivity PEDOT:PSS transparent electrodes for stretchable and mechanically-robust organic solar cells. *Solar Energy Materials and Solar Cells, 110*, 98–106. [CrossRef]

[29] He, J., Gao, P., Ling, Z., Ding, L., Yang, Z., Ye, J., & Cui, Y. (2016). High-efficiency silicon/organic heterojunction solar cells with improved junction quality and interface passivation. *ACS nano, 10*(12), 11525-11531. [CrossRef]

[30] Yu, Z., Xia, Y., Du, D., & Ouyang, J. (2016). PEDOT: PSS films with metallic conductivity through a treatment with common organic solutions of organic salts and their application as a transparent electrode of polymer solar cells. *ACS applied materials & interfaces, 8*(18), 11629-11638. [CrossRef]

[31] Zhang, Y., Zu, F., Lee, S.-T., Liao, L., Zhao, N., & Sun, B. (2014). Heterojunction with organic thin layers on silicon for record efficiency hybrid solar cells. *Advanced Energy Materials, 4*(2), 1300923. [CrossRef]

[32] Yu, P., Tsai, C. Y., Chang, J. K., Lai, C. C., Chen, P. H., Lai, Y. C., ... & Meng, H. F. (2013). 13% efficiency hybrid organic/silicon-nanowire heterojunction solar cell via interface engineering. *ACS nano, 7*(12), 10780-10787. [CrossRef]

[33] Zhu, Z., Liu, C., Xu, J., Jiang, Q., Shi, H., & Liu, E. (2016). Improving the electrical conductivity of PEDOT:PSS films by binary secondary doping. *Electronic Materials Letters, 12*(1), 54–58. [CrossRef]

[34] Schmidt, J., Titova, V., & Zielke, D. (2013). Organic-silicon heterojunction solar cells: Open-circuit voltage potential and stability. *Applied Physics Letters, 103*(18), 183901. [CrossRef]

[35] Iqbal, S., Iqbal, M., Yang, Z., Guo, X., & Zhang, T. (2026, May). Spectral Management in Organic-Si Heterojunction Solar Cells via Dual-Layer Architecture for Enhanced Charge Extraction and Optical Optimization. In *Innovative Approaches for Global Sustainability: Selected Papers from the 2025 International Conference on Sustainable Innovations and Partnerships (SIP 2025)* (pp. 27-40). Cham: Springer Nature Switzerland. [CrossRef]

[36] Iqbal, S., Yang, Y., Su, D., Yang, Z., Guo, X., & Zhang, T. (2025). Tailored spectral management in PEDOT: PSS-based organic-Si heterojunction solar cells via dual-layer architecture for enhanced charge extraction and optical optimization. *Optical and Quantum Electronics, 58*(1), 45. [CrossRef]

Appendix

A1. Device-level photovoltaic parameters

Table A1 lists the individual devices behind the statistics in Figure A1. Single-layer (SL) devices were prepared with 5 wt% DMSO or 7 wt% EG only; dual-layer (DL) devices use the EG (7 wt%) bottom layer and the DMSO (5 wt%) top layer.

Table A1. Photovoltaic parameters of individual single-layer (SL) and dual-layer (DL) PEDOT:PSS/n-Si devices.

No.	Device architecture	V_{oc} (mV)	J_{sc} (mA cm^{-2})	FF (%)	PCE (%)
1	SL-DMSO [5 wt%]	428.3	5.96	38.7	0.98
2	SL-DMSO [5 wt%]	506.0	15.5	38.7	3.30
3	SL-EG [7 wt%]	425.7	5.67	39.01	1.03
4	SL-EG [7 wt%]	509.1	14.3	50.1	3.13
5	DL-EG:DMSO [7 wt% | 5 wt%]	598.1	15.7	58.0	5.10
6	DL-EG:DMSO [7 wt% | 5 wt%]	604.5	16.57	61.03	5.91
7	DL-EG:DMSO [7 wt% | 5 wt%]	607.8	16.13	56.7	5.73
8	DL-EG:DMSO [7 wt% | 5 wt%]	505.7	18.1	53.6	4.92

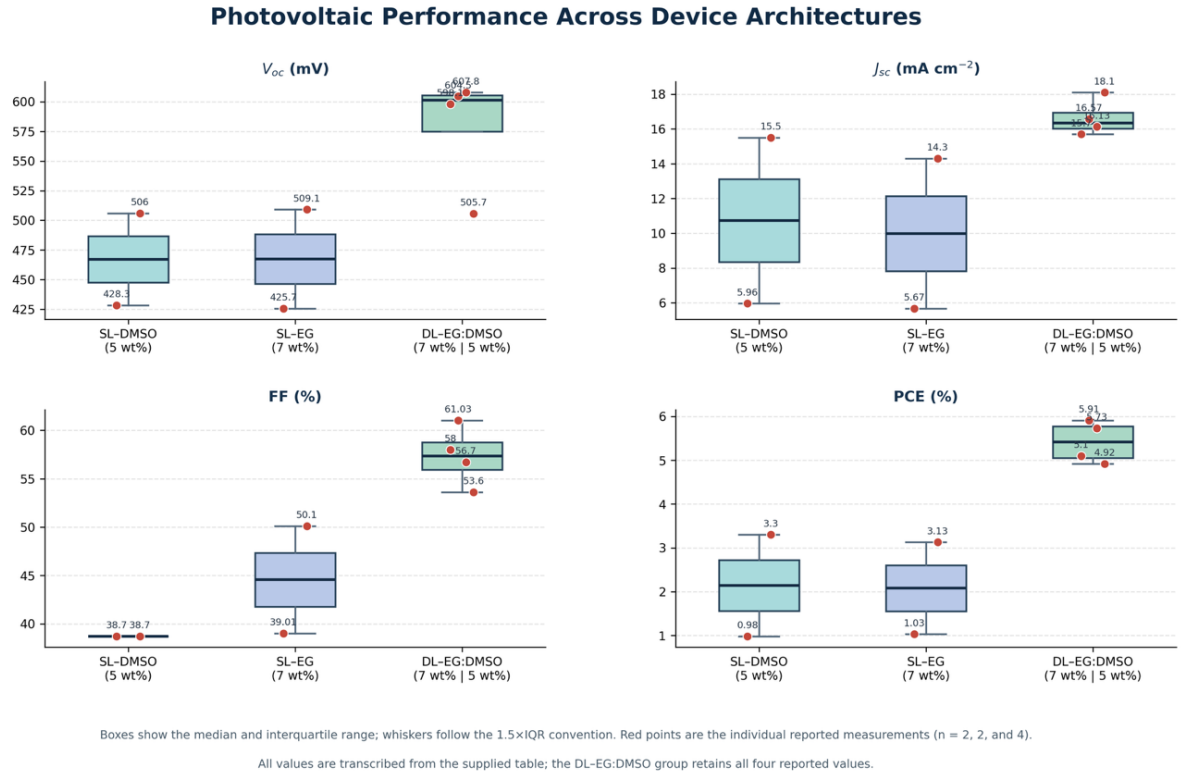

Figure A1. Photovoltaic parameters (V_{oc}, J_{sc}, FF, PCE) of the three device architectures. Boxes show the median and interquartile range, whiskers follow the 1.5×IQR convention, and points are individual devices (n = 2, 2 and 4).

A2. Statement of novelty relative to earlier bilayer PEDOT:PSS work

Dual-layer PEDOT:PSS films on silicon have been reported before [26]. What differs here is the choice of a different secondary dopant for each layer:

1. *Separate roles for the two co-solvents.* The bottom layer contains EG (7 wt%) and is intended to promote adhesion and contact with n-Si; the top layer contains DMSO (5 wt%) and is intended to supply conductivity for carrier extraction. These roles are taken from the secondary-doping literature and are not isolated by separate control experiments in this work.

2. *Surface-potential uniformity.* KPFM (Figure 6 for the dual-layer film and Figure A3 for the single-layer film) was used to examine the contact potential difference (CPD) and its gradient $|\nabla V|$ across the film surface.

3. *Efficiency.* The best dual-layer device reached a PCE of 6.96%, compared with 3.27% for the single-layer reference (Table 1).

A3. AFM and KPFM of the single-layer device

Figure A2 shows the AFM topography of the single-layer film, from which the roughness values quoted in the main text were taken for comparison with the dual-layer film (Figure 8); the corresponding KPFM results are shown in Figure A3.

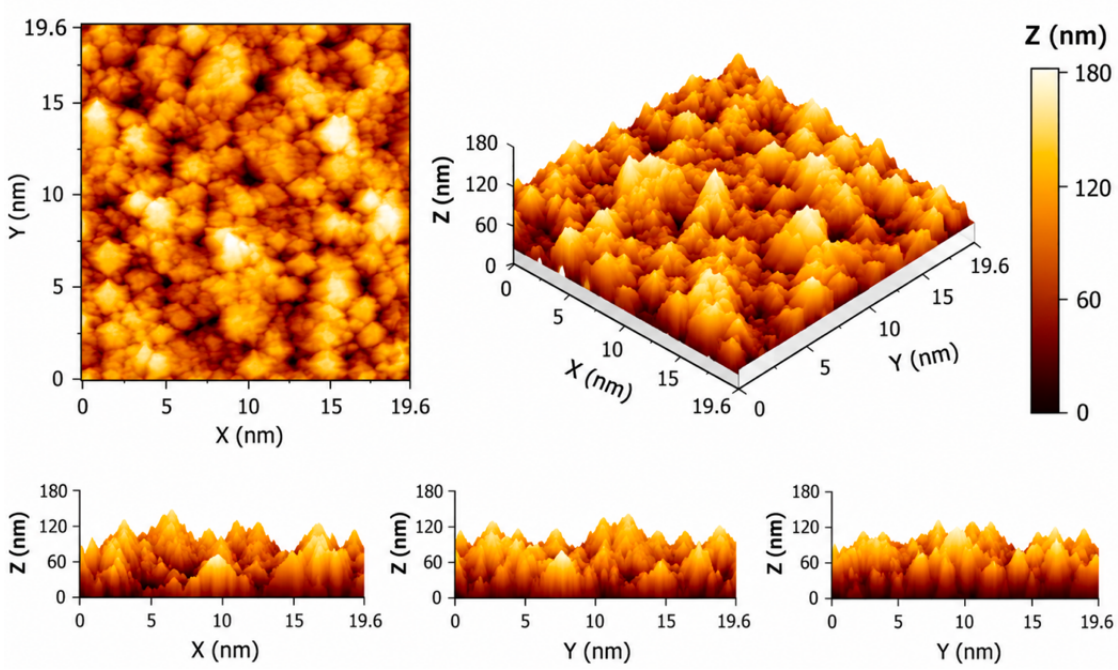

Figure A2. AFM topography of the single-layer device: two-dimensional image, three-dimensional view and line profiles along X and Y (height scale 0–180 nm).

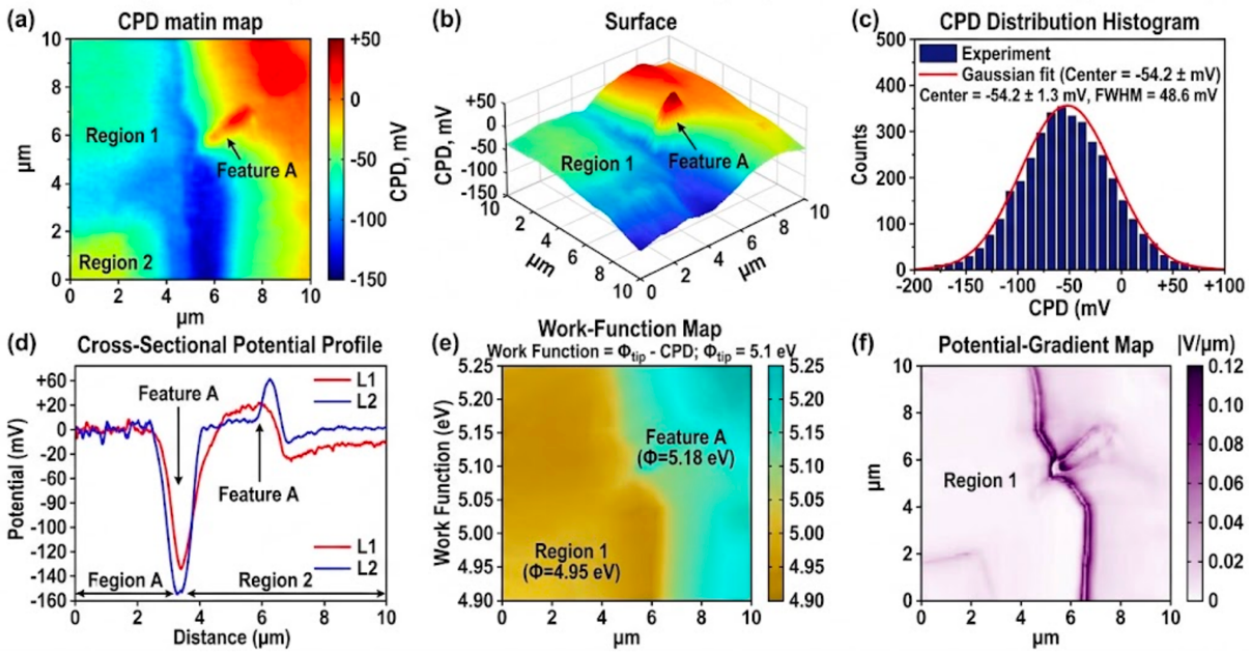

Figure A3. KPFM of the single-layer device. (a) CPD map, (b) three-dimensional CPD surface, (c) CPD histogram with Gaussian fit (center -54.2 ± 1.3 mV, FWHM 48.6 mV), (d) cross-sectional potential profiles along lines L1 and L2, (e) work-function map ($\Phi = \Phi_{\mathrm{tip}} - \mathrm{CPD}$, $\Phi_{\mathrm{tip}} = 5.1$ eV), (f) potential-gradient map $|\nabla V|$.